Solar Energy Materials & Solar Cells 164 (2017) 28–31

Contents lists available at ScienceDirect

Solar Energy Materials & Solar Cells

journal homepage: www.elsevier.com/locate/solmat

Absorption coefficients in AlGaInP lattice-matched to GaAs

J.S. Cheong, A.N.A.P. Baharuddin, J.S. Ng, A.B. Krysa, J.P.R. David*

Department of Electronic and Electrical Engineering, University of Sheffield, Sheffield S3 7HQ United Kingdom

ARTICLE INFO

Keywords:
Absorption coefficient
Diffusion length
GaInP
AlGaInP
AlInP
Bandgap

ABSTRACT

The absorption coefficient of AlGaInP lattice-matched to GaAs, across the composition range from AlInP to GaInP has been obtained from photocurrent versus wavelength measurements on seven homo-junction AlGaInP PIN diode structures. Due to the sensitivity of the photocurrent measurement technique, values of absorption down to 10^0 cm^{-1} have been determined close to the band-gap. From these, the bandgaps in this material system were extracted across the composition range and these corroborate data in the literature that shows the band-gap becoming indirect when the aluminium content, $x > 0.48$.

1. Introduction

The quaternary alloy $(Al_xGa_{1-x})_{0.52}In_{0.48}P$ (hereafter referred to as AlGaInP) is an attractive material for solar cell applications. Due to the bandgap tunability of the quaternary alloy while being lattice-matched to GaAs, it has been used extensively as the absorber material or as an optical window in solar cells [1–4] where efficiencies of >40% have been obtained. Designs of such devices require an accurate knowledge of the absorption coefficient, α, as a function of wavelength, λ, across the alloy composition. This is important to optimise the energy conversion efficiency due to the ability to absorb shorter wavelength photons, and to accurately determine any losses in the window region.

There are several experimental methods for measuring $\alpha(\lambda)$ in a semiconductor. Kato et al. [5] have reported $\alpha(\lambda)$ of AlGaInP over a wide wavelength range using ellipsometric techniques, by extracting both the refractive index, n, and extinction coefficient, k. However the reliability of the measurement primarily depends on the surface quality of the semiconductors and it was shown that the optical constants at the absorption band edge can vary considerably due to surface roughness and the presence of native oxides [5]. This prevents the precise measurement of $\alpha < 10^4$ cm^{-1}, in addition to limits imposed by the ellipsometer's inherent accuracy [6]. Although these values of α are relatively low, it can be critical in estimating the efficiency of solar cells with light trapping abilities [7], as well as in accurately determining the loss of any window layers [2,3]. One way to obtain lower values of α is via a transmission measurement technique, which gives a good estimation of α down to 10^0 cm^{-1} within an uncertainty of ~20% [8]. A wide dynamic range of α from 10^6 to 10^0 cm^{-1} is usually achieved by merging the data obtained from both transmission and ellipsometry measurements [9–11]. However, such a technique is difficult to perform on AlGaInP alloys as the lattice matched GaAs substrate is opaque at the wavelengths of interest and therefore has to be removed prior to any transmission measurement.

An alternative method of determining the absorption coefficients is by obtaining the spectral quantum efficiencies from photocurrent measurements in PIN diodes [12]. Provided the structure used is appropriately designed, this technique can give accurate values of $\alpha(\lambda)$ over a wide dynamic range. The changes in doping within parts of the PIN diode should not pose a problem as α is relatively insensitive to even moderately high doping densities of $< 2\times10^{18}$ cm^{-3} [13,14]. In this paper, we use this method to obtain $\alpha(\lambda)$ for AlGaInP alloys, over its entire composition range from AlInP to GaInP.

2. Device growth, fabrication and characterization

A series of seven AlGaInP homo-junction PIN diodes (across the entire composition range of GaInP to AlInP) with nominal intrinsic region thickness, w of 1.0 μm, was used for this work. All wafers were grown on 10° off-axis n^+ GaAs substrates by metal-organic-chemical-vapor deposition (MOCVD) to minimise the effects of Cu-Pt ordering [15] and the consequent reduction in band-gap. A summary of the wafers used in this study is given in Table 1. The AlInP PIN (x=1.0) was grown previously and was reported as P2-1 in an earlier publication [12]. The p^+ and n^+ cladding layers nominal thicknesses were 1.0 and 0.3 μm respectively and the top AlGaInP p^+ was finally capped with a 50 nm thin p^+ GaAs to ensure a good ohmic contact as shown in Table 1.

Double crystal X-ray rocking curves (XRD) (not shown here) revealed that the lattice mismatch between AlGaInP and GaAs is minimal for all these structures at $< \pm 2\times10^{-3}$. The measured alumi-

* Corresponding author.
E-mail address: j.p.david@sheffield.ac.uk (J.P.R. David).

http://dx.doi.org/10.1016/j.solmat.2017.01.042
Received 29 September 2016; Received in revised form 10 January 2017; Accepted 27 January 2017
Available online 10 February 2017
0927-0248/

Table 1
Nominal structure details of AlGaInP diodes grown on 10° off-axis n^+ GaAs substrate, described from top to bottom.

Purpose	Thickness (μm)	Material
Cap	0.05	GaAs
p^+ cladding	1.0	AlGaInP
Intrinsic	1.0	AlGaInP
n^+ cladding	0.3	AlGaInP
n^+ cladding	0.3	GaAs

nium compositions in these samples are shown in Table 2. Circular mesa diodes (35 – 210 μm radii) with annular top contacts were fabricated using standard photolithography and wet chemical etching as detailed in [12]. To minimise undesirable light absorption within the 50 nm GaAs cap, it was removed by wet chemical etching in the window region. The mesa sidewalls were passivated using SU-8 and covered with gold to ensure that any photocurrent measured was only due to light falling on the optical window region. Due to the large bandgap in these samples, the dark currents were < 5 pA at −5 V even in the largest radii devices and were found to be < 3 μA cm^{-2} at 95% of their respective breakdown voltages.

Capacitance-voltage (*C-V*) measurements were performed on the devices to extract the depletion widths, w and the doping densities of the cladding layers using dielectric constants which are interpolated from GaP, InP and AlP, given as 11.2 [16], 12.6 [17] and 9.8 [18] respectively. The n^+ cladding layers were silicon doped to a level of ~2×10^{18} cm^{-3} for all alloy compositions [19]. The doping densities in the p^+ and i regions were obtained by modelling the *C-V* results (see Fig. 1) assuming an n^+ layer doping of 2×10^{18} cm^{-3}. The p^+ cladding doping densities in all the samples were found to be approximately between 2×10^{17} cm^{-3} and 2×10^{18} cm^{-3} as shown in Table 1. This doping level generally decreases as the aluminium fraction in the sample increases due to the decreasing solubility of the zinc dopants [20]. The thickness of the intrinsic region, w in these devices are determined as 0.93–1.00 μm, except for the previously grown AlInP PIN, which was 1.14 μm.

3. Results and discussion

A 100 W tungsten bulb and a grating monochromator were used to measure the spectral responses in the largest diameter devices. The effect of any Franz-Keldysh electro-absorption [21,22] on the photocurrent was assumed minimal as all measurements were undertaken at 0 V. Using a calibrated silicon photodiode as reference, the experimental spectral responses yielded quantum efficiencies (η) of the devices over three orders of magnitude due to the very low dark currents of these devices, as shown in Fig. 2. The quantum efficiency data were also corroborated using either a 442 nm He-Cd or 543 nm He-Ne laser (whichever gave the larger photocurrent in these devices), where the laser beam was focused to a 20 μm diameter spot on the device optical window.

A one-dimensional quantum efficiency model derived using the current continuity equation [23] was used to extract $\alpha(\lambda)$ from the

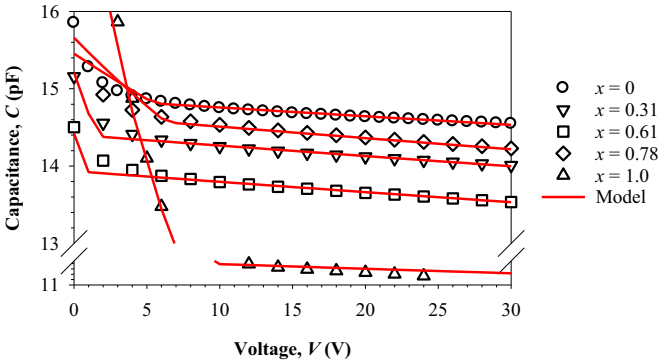

Fig. 1. Measured (symbols) and modelled (lines) capacitance of AlGaInP (x=0, 0.31, 0.61, 0.78, 1.00) shown as ○, ▽, □ , ◇ and Δ respectively. Results for x=0.47 and 0.64 are omitted for clarity.

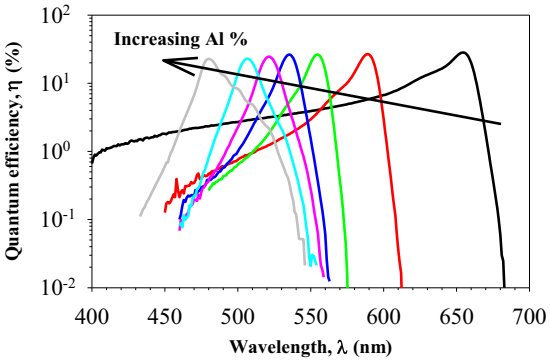

Fig. 2. Quantum efficiency determined from measured spectral responses in the AlGaInP PINs (x=0, 0.31, 0.47, 0.61, 0.64, 0.78 and 1.00). Data shown for AlInP was obtained from [12].

experimental $\eta(\lambda)$ in these samples. The parameter η is the sum of the efficiency contributed by carriers generated in the p^+, i and n^+ AlGaInP layers, i.e. η_p, η_i and η_n respectively, which can be expressed as

$$\eta = (1 - R)\left(\eta_p + \eta_i + \eta_n\right). \quad (1)$$

where R is the reflectivity of the semiconductor surface. Any carriers created in the underlying n^+ GaAs will not contribute to the photocurrent as GaAs-AlGaInP has a Type I band offset [24]. The usual expressions for η_p, η_i and η_n from [23] are given in Eqs. (2)–(4). This requires knowledge of L_e (L_h), D_e (D_h) and S_e (S_h) which are the diffusion lengths, diffusion coefficients and surface recombinations respectively. X_1 and X_2 are the distances from the top surface to the depletion edge in the p^+ and n^+ region respectively and X_3 is the total thickness of the three AlGaInP layers. These thicknesses can be estimated accurately from the epitaxial growth rates and *C-V* measurements.

In order to obtain L_e, we measure the photocurrent at a fixed wavelength as a function of the reverse bias voltage. Due to the unpassivated semiconductor surface in the window region, S_e can

Table 2
device parameters of AlGaInP Diodes.

Al fraction	w (μm) ± 0.01 μm	N_p ($\times10^{17}$ cm^{-3}) ± 1×10^{17} cm^{-3}	N_i ($\times10^{15}$ cm^{-3}) ± 1×10^{15} cm^{-3}	L_e (μm) ± 5%
0.00	0.97	18	2	0.27
0.31	0.99	10	2	0.25
0.47	0.93	9	3	0.22
0.61	1.00	8	2	0.20
0.64	0.96	8	2	0.20
0.78	0.94	10	2	0.15
1.00	1.14	3	7	0.15

be assumed to be large at ~1×10^{7} cm s^{-1} [25] in all samples and

$$\eta_p = \left[\frac{\alpha L_e}{\alpha^2 {L_e}^2 - 1}\right]\left[\frac{\frac{S_e L_e}{D_e} + \alpha L_e - \exp(-\alpha X_1)\left(\frac{S_e L_e}{D_e}\cosh\left(\frac{X_1}{L_e}\right) + \sinh\left(\frac{X_1}{L_e}\right)\right)}{\frac{S_e L_e}{D_e}\sinh\left(\frac{X_1}{L_e}\right) + \cosh\left(\frac{X_1}{L_e}\right)} - \alpha L_e \exp(-\alpha X_1)\right] \quad (2)$$

$$\eta_i = (\exp[-\alpha X_1])(1 - \exp[-\alpha(X_2 - X_1)]) \quad (3)$$

$$\eta_n = \left[\frac{\alpha L_h}{\alpha^2 {L_h}^2 - 1}\right][\exp[-\alpha(X_3 - X_2)]] \times \left[\alpha L_h - \frac{\frac{S_h L_h}{D_h}\left[\cosh\left(\frac{X_3}{L_h}\right) - \exp(-\alpha X_3)\right] + \sinh\left(\frac{X_3}{L_h}\right) + \alpha L_h \exp(-\alpha X_3)}{\frac{S_h L_h}{D_h}\sinh\left(\frac{X_3}{L_h}\right) + \cosh\left(\frac{X_3}{L_h}\right)}\right] \quad (4)$$

therefore Eq. (2) approaches to

$$\eta_p = \left[\frac{\alpha L_e}{\alpha^2 {L_e}^2 - 1}\right]\left[\frac{1}{\sinh\left(\frac{X_1}{L_e}\right)} - \alpha L_e \exp(-\alpha X_1)\right]. \quad (5)$$

By choosing a short enough wavelength (that varied between 442 and 532 nm for the different compositions), we can ensure that the light is almost entirely absorbed in the p^+ cladding layer while providing a measurable photocurrent, and therefore, Eq. (1) becomes η=(1-R)η_P. The short wavelength also ensures the product of αX_1 is large and Eq. (5) can then be further simplified to

$$\eta_p \propto \frac{1}{\cosh\left(\frac{X_1}{L_e}\right)}. \quad (6)$$

With increasing reverse bias, X_1 decreases and η_P increases almost linearly as described by Woods et al. [26]. Using Eq. (6), L_e was extracted from the experiment data of short wavelength photocurrent versus reverse bias voltage as shown in Fig. 3 and the values obtained are shown in Table 1. For clarity, only data from samples with aluminium fraction of 0, 0.47 and 1.00 are shown here.

In Table 1, L_e is fairly short and decreases with increasing aluminium fraction, similar to the trend found in AlGaAs by Hooft et al. [27]. This may be due to increasing trap and defect densities with aluminium content. The GaInP sample has the longest L_e, and consequently the highest peak η of 28.2% which is consistent with results in [2,28].

Due to the thickness of the p^+ and i regions, the carriers created in the bottom n^+ AlGaInP makes only a minor contribution to the photocurrent measured especially when the absorption coefficient is

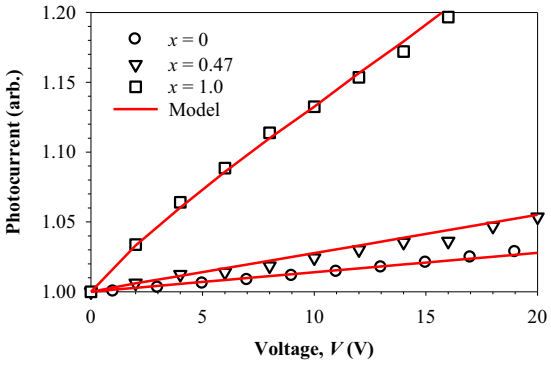

Fig. 3. Measured (symbols, with an accuracy of ± 2.5%) and modelled (lines) photocurrent as a function of bias voltage in x=0, 0.47 and 1.00 shown as ○, ▽, □ respectively.

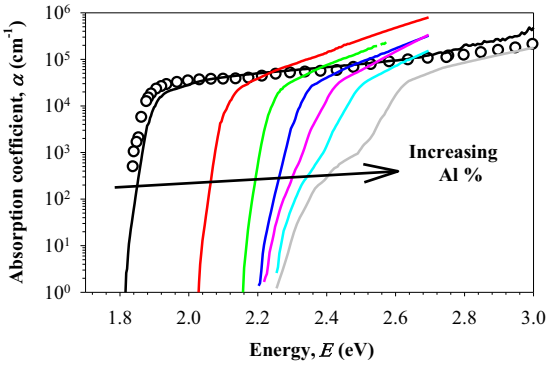

Fig. 4. Absorption coefficients in AlGaInP PINs (x=0, 0.31, 0.47, 0.61, 0.64, 0.78 and 1.00) as deduced from the QE measurements of Fig. 3. GaInP absorption data from Schubert et. al. [29] (○) is also included.

large. At longer wavelengths and low values of absorption coefficient, some carriers are generated in the n^+ layer and this is taken into account by assuming that S_h=S_e (due to the bottom n^+ AlGaInP/ n^+ GaAs heterojunction) and by L_h =L_e.

Using the determined L_e's shown in Table 1 along with other parameters as discussed in the above paragraph, the absorption coefficients were determined from the measured η as shown in Fig. 4 after calculating the surface reflectivity in these samples using

$$R(\lambda) = \frac{[n(\lambda) - 1]^2 + k^2(\lambda)}{[n(\lambda) + 1]^2 + k^2(\lambda)}, \quad (7)$$

where k is related to α via $k = \frac{\alpha\lambda}{4\pi}$.

The refractive indices in these materials were obtained by linearly interpolating the experimental results from Kato et al. [5]. The α extracted from GaInP gives excellent agreement with that of Schubert et al. [29] (calculated from k) over a wide range of wavelength down to < 450 nm. It is clear from Fig. 4 that the AlGaInP absorption curves blue-shift with increasing aluminium fraction. The increase in α with increasing photon energy, E above the bandgap in the quaternary alloys and AlInP is distinctly different from that of GaInP, however appears to be similar to that reported in Si [30] and AlGaAs [31]. A detailed explanation for the behaviour of α above the band-gap in this alloy system is beyond the scope of this experimental study.

The α's were used to determine the Γ energy gap, E_Γ of these alloys by obtaining the x-intercept from α^2 versus energy plot [32] as illustrated in Fig. 5. The indirect band-gap, E_x was obtained by plotting $\alpha^{0.5}$ versus energy [32] in a similar manner in Fig. 5. The absorption tails which occurs below the band-gap as shown in Fig. 5 are primarily associated with the Urbach tail which arises due to structural and thermal disorder [22]. The energy gaps determined in these samples are summarized in Fig. 6 and are in excellent agreement with those of Mowbray et al. [33] (where the reported 4 K data was converted to 300 K data by subtracting 80 meV). E_Γ and E_x can be expressed as a function of aluminium fraction, x as E_Γ (x)=1.899+0.704x and E_x≈2.24 eV respectively with the direct-indirect crossover occurring at 0.48. Using the extracted α's, it is now feasible to model the efficiency of AlGaInP multi-junction solar cells which utilise different alloy compositions in absorber and window layers with improved accuracy over a wide spectral range.

4. Conclusion

The spectral responses of a series of seven AlGaInP PINs lattice matched to GaAs across the entire alloy range were measured and from their quantum efficiency, the absorption coefficients over five orders of magnitude were extracted accurately down to values as low as 10^0 cm^{-1}. The values of the direct and indirect gaps obtained from the absorption coefficients are in good agreement with those published

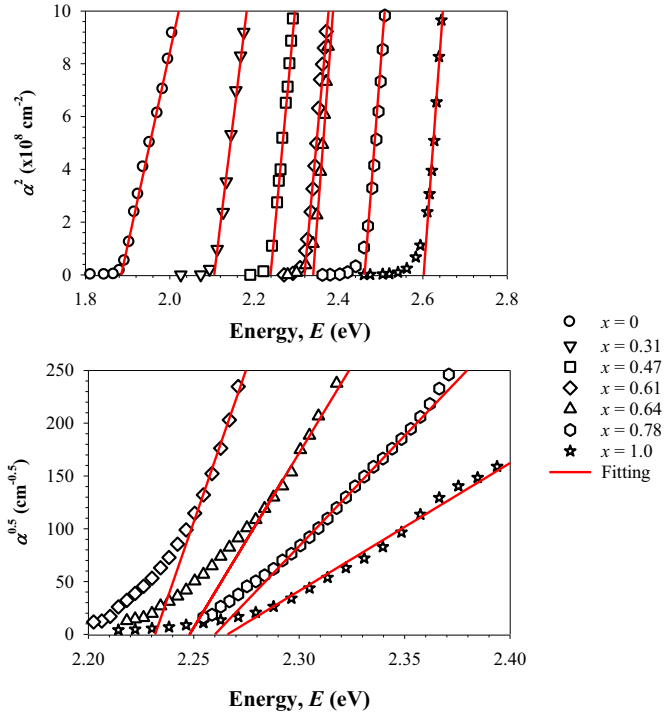

Fig. 5. Extracting the direct (top) and indirect energy gaps (bottom) of AlGaInP by fitting (lines) to experimental values (x=0, 0.31, 0.47, 0.61, 0.64, 0.78 and 1.00) shown as ○, ▽, □, ◇, △,⬡ and ☆ respectively of absorption coefficient.

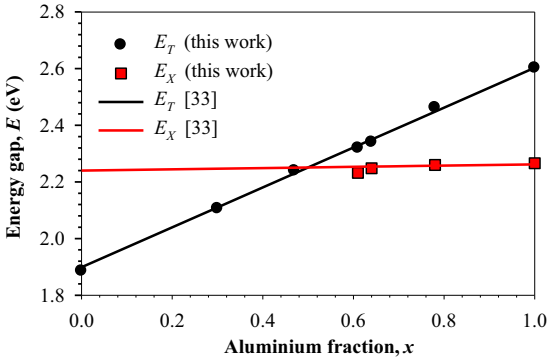

Fig. 6. Measured direct and indirect gaps of AlGaInP as a function of aluminium fraction shown as ○ and □ respectively. The solid black and red lines are direct and indirect gaps obtained from [33].

in the literature with the material system becoming indirect for aluminium compositions > 0.48.

Acknowledgement

This work was supported by the U.K. Engineering and Physical Sciences Research Council (EPSRC), Grant No. EP/K001469/1.

The author A. N. A. P Baharuddin would like to thank the Malaysia People's Trust Council and the University of Kuala Lumpur, for the scholarship.

References

[1] R.R. King, D. Bhusari, D. Larrabee, X.Q. Liu, E. Rehder, K. Edmondson, H. Cotal, R.K. Jones, J.H. Ermer, C.M. Fetzer, D.C. Law, N.H. Karam, Solar cell generations over 40% efficiency, Prog. Photovolt.: Res. Appl. 20 (2012) 801–815.

[2] E.E. Perl, J. Simon, J.F. Geisz, W. Olavarria, M. Young, A. Duda, D.J. Friedman, M.A. Steiner, Development of high-bandgap AlGaInP solar cells grown by organometallic vapor-phase epitaxy, IEEE J. Photovolt. 6 (2016) 770–776.

[3] H. Lu, X. Li, W. Zhang, D. Zhou, M. Shi, L. Sun, K. Chen, A 2.05 eV AlGaInP sub-cell used in next generation solar cells, J. Semicond. 35 (2014) 094010.

[4] A.B. Cornfeld, P. Patel, J. Spann, D. Aiken, J. McCarty, Evolution of a 2.05 eV AlGaInP top sub-cell for 5 and 6J-IMM applications, in: Proceedings of the 38th IEEE Photovoltaic Specialists Conference (PVSC), 2012, pp. 002788–002791.

[5] H. Kato, S. Adachi, H. Nakanishi, K. Ohtsuka, Optical Properties of (Al_xGa_{1-x}) $0.5In_{0.5}P$ Quaternary Alloys, Jpn. J. Appl. Phys. 33 (1994) 186–192.

[6] F. Lukeš, The accuracy of the measurement of the ellipsometric parameters Δ and ψ, Surf. Sci. 16 (1969) 74–84.

[7] S. Mokkapati, K.R. Catchpole, Nanophotonic light trapping in solar cells, J. Appl. Phys. 112 (2012) 101101.

[8] G.G. Macfarlane, V. Roberts, Infrared absorption of germanium near the lattice edge, Phys. Rev. 97 (1955) 1714–1716.

[9] W.C. Dash, R. Newman, Intrinsic optical absorption in single-crystal germanium and silicon at 77 K and 300 K, Phys. Rev. 99 (1955) 1151–1155.

[10] H.R. Philipp, E.A. Taft, Optical constants of germanium in the region 1 to 10 ev, Phys. Rev. 113 (1959) 1002–1005.

[11] H.R. Philipp, E.A. Taft, Optical constants of silicon in the region 1 to 10 ev, Phys. Rev. 120 (1960) 37–38.

[12] J.S. Cheong, J.S. Ng, A.B. Krysa, J.S.L. Ong, J.P.R. David, Determination of absorption coefficients in AlInP lattice matched to GaAs, J. Phys. D: Appl. Phys. 48 (2015) 405101.

[13] H.C. Casey, D.D. Sell, K.W. Wecht, Concentration dependence of the absorption coefficient for n– and p–type GaAs between 1.3 and 1.6 eV, J. Appl. Phys. 46 (1975) 250–257.

[14] G.E. Jellison, F.A. Modine, C.W. White, R.F. Wood, R.T. Young, Optical properties of heavily doped silicon between 1.5 and 4.1 eV, Phys. Rev. Lett. 46 (1981) 1414–1417.

[15] L.C. Su, I.H. Ho, G.B. Stringfellow, Effects of substrate misorientation and growth rate on ordering in GaInP, J. Appl. Phys. 75 (1994) 5135–5141.

[16] D.J. Lockwood, G. Yu, N.L. Rowell, Optical phonon frequencies and damping in AlAs, GaP, GaAs, InP, InAs and InSb studied by oblique incidence infrared spectroscopy, Solid State Commun. 136 (2005) 404–409.

[17] L.G. Meiners, Temperature dependence of the dielectric constant of InP, J. Appl. Phys. 59 (1986) 1611–1613.

[18] B. Monemar, Determination of band gap and refractive index of AIP from optical absorption, Solid State Commun. 8 (1970) 1295–1298.

[19] K.A. Bertness, S.R. Kurtz, S.E. Asher, R.C. Reedy Jr, AlInP benchmarks for growth of AlGaInP compounds by organometallic vapor-phase epitaxy, J. Cryst. Growth 196 (1999) 13–22.

[20] Y. Ohba, Y. Nishikawa, C. Nozaki, H. Sugawara, T. Nakanisi, A study of p-type doping for AlGaInP grown by low-pressure MOCVD, J. Cryst. Growth 93 (1988) 613–617.

[21] L.V. Keldysh, Behaviour of non-metallic crystals in strong electric fields, J. Exp. Theor. Phys. 33 (1957).

[22] F. Urbach, The Long-wavelength edge of photographic sensitivity and of the electronic absorption of solids, Phys. Rev. 92 (1953) (1324-1324).

[23] H.J. Hovel, R.K. Willardson, A.C. Beer, Semiconductors and Semimetals 11, Academic Press, New York, 1975.

[24] M.O. Watanabe, Y. Ohba, Interface properties for GaAs/InGaAlP heterojunctions by the capacitance-voltage profiling technique, Appl. Phys. Lett. 50 (1987) 906–908.

[25] D. Bimberg, M. Grundmann, N.N. Ledentsov, Quantum Dot Heterostructures, Wiley, 1999.

[26] M.H. Woods, W.C. Johnson, M.A. Lampert, Use of a Schottky barrier to measure impact ionization coefficients in semiconductors, Solid-State Electron. 16 (1973) 381–394.

[27] G.W. Hooft, C. van Opdorp, H. Veenvliet, A.T. Vink, Minority carrier lifetime and luminescence in MOVPE-grown (Al,Ga)As epilayers and DH lasers, J. Cryst. Growth 55 (1981) 173–182.

[28] T. Masuda, S. Tomasulo, J.R. Lang, M.L. Lee, Comparison of single junction AlGaInP and GaInP solar cells grown by molecular beam epitaxy, J. Appl. Phys. 117 (2015) 094504.

[29] M. Schubert, V. Gottschalch, C.M. Herzinger, H. Yao, P.G. Snyder, J.A. Woollam, Optical constants of GaxIn1−xP lattice matched to GaAs, J. Appl. Phys. 77 (1995) 3416–3419.

[30] M.A. Green, Self-consistent optical parameters of intrinsic silicon at 300 K including temperature coefficients, Sol. Energy Mater. Sol. Cells 92 (2008) 1305–1310.

[31] D.E. Aspnes, S.M. Kelso, R.A. Logan, R. Bhat, Optical properties of AlxGa1−xAs, J. Appl. Phys. 60 (1986) 754–767.

[32] L. Hall, J. Bardeen, F. Blatt, Infrared absorption spectrum of germanium, Phys. Rev. 95 (1954) 559.

[33] D.J. Mowbray, O.P. Kowalski, M. Hopkinson, M.S. Skolnick, J.P.R. David, Electronic band structure of AlGaInP grown by solid-source molecular-beam epitaxy, Appl. Phys. Lett. 65 (1994) 213–215.